Author Manuscript

Author Manuscript

Author Manuscript

Author Manuscript

HHS Public Access

Author manuscript

Dev Biol. Author manuscript; available in PMC 2017 October 10.

Published in final edited form as:

Dev Biol. 2017 October 01; 430(1): 214–223. doi:10.1016/j.ydbio.2017.07.018.

Trinucleotide repeat containing 6c (TNRC6c) is essential for microvascular maturation during distal airspace sacculation in the developing lung

Hua Guo[a,1], **Yana Kazadaeva**[b,1], **Fabian E. Ortega**[c], **Narasimaswamy Manjunath**[a], **Tushar J. Desai**[b,*]

[a]Center of Emphasis in Infectious Disease, Department of Biomedical Sciences, Texas Tech University Health Sciences Center, El Paso, TX 79905, United States

[b]Department of Internal Medicine, Division of Pulmonary and Critical Care, Stanford University School of Medicine, Stanford, CA 94305, United States

[c]Department of Biochemistry, Stanford University School of Medicine, Stanford, CA 94305, United States

Abstract

GW182 (also known asTNRC6) family members are critically involved in the final effector phase of miRNA-mediated mRNA repression. The three mammalian paralogs, TNRC6a, b and c, are thought to be redundant based on Argonaute (Ago) binding, tethering assays, and RNAi silencing of individual members in cell lines. To test this idea, we generated TNRC6a, b and c knockout mice. TNRC6a mutants die at mid-gestation, while b-and c- deleted mice are born at a Mendelian ratio. However, the majority of TNRC6b and all TNRC6c mutants die within 24 h after birth, the latter with respiratory failure. Necropsy of TNRC6c mutants revealed normal-appearing airways that give rise to abnormally thick-walled distal gas exchange sacs. Immunohistological analysis of mutant lungs demonstrated a normal distribution of bronchiolar and alveolar cells, indicating that loss of TNRC6c did not abrogate epithelial cell differentiation. The cellular kinetics and relative proportions of endothelial, epithelial, and mesenchymal cells were also not altered. However, the underlying capillary network was simplified and endothelial cells had failed to become tightly apposed to the surface epithelium in TNRC6c mutants, presumably causing the observed respiratory failure. TGFβ family mutant mice exhibit a similar lung phenotype of thick-walled air sacs and neonatal lethality, and qRT-PCR confirmed dynamic downregulation of TGFβ1 and TGFβR2 in TNRC6c mutant lungs during sacculation. VEGFR, but not VEGF-A ligand, was also lower, likely reflecting the overall reduced capillary density in TNRC6c mutants. Together, these results demonstrate that GW182 paralogs are not functionally redundant in vivo. Surprisingly, despite regulating a general cellular process, TNRC6c is selectively required only in the distal lung and not until late in gestation for proper expression of the TGFβ family genes that drive

This is an open access article under the CC BY-NC-ND license (http://creativecommons.org/licenses/BY-NC-ND/4.0/).

*Corresponding author. tdesai@stanford.edu (T.J. Desai).

[1]Equal contribution.

Appendix A. Supporting information

Supplementary data associated with this article can be found in the online version at doi:10.1016/j.ydbio.2017.07.018.

Author Manuscript Author Manuscript Author Manuscript Author Manuscript

sacculation. These results imply a complex and indirect mode of regulation of sacculation by TNRC6c, mediated in part by dynamic transcriptional repression of an inhibitor of TGFβ family gene expression.

Keywords

TNRC6; TGFβ; Sacculation; Lung alveolar development; MiRNA; Microvascular immaturity

1. Introduction

MicroRNAs (miRNAs) are small 22 nucleotide (nt) double stranded RNAs that serve as key regulators of gene expression in many cellular pathways. They are initially transcribed as long primary miRNAs that are processed in the nucleus by drosha/DGCR8 into ~70 nt hairpin structures called pre-miRNAs (reviewed in Bartel (2004), Carthew and Sontheimer (2009), Manjunath et al. (2009), Murchison and Hannon (2004)). Pre-miRNAs are exported to the cytoplasm where they undergo additional processing by Dicer to generate mature miRNAs that are loaded onto a protein complex called RNA-induced silencing complex (RISC), where the miRNA directly interacts with a member of the Argonaute family of proteins (Ago1–4) (Dueck and Meister, 2014; Kawamata and Tomari, 2010). Each miRNA, which is typically partially complementary to target sites (at nts 2–8, known as the seed sequence) in the 3′ UTR, guides the RISC to its target mRNA (Doench and Sharp, 2004; Lewis et al., 2003). Upon miRNA binding its target mRNA, the Ago protein recruits a member of the GW182 (also known as trinucleotide repeat containing 6, TNRC6) protein family and the entire complex localizes in discrete cytoplasmic foci called GW or P-bodies. GW182 is characterized by the presence of glycine-tryptophan (GW) repeats at the N-terminus that provide the binding site for Ago proteins (Baillat and Shiekhattar, 2009; Eulalio et al., 2008; Lian et al., 2009; Takimoto et al., 2009). The C-terminus of GW182 proteins may be considered the silencing domain because it coordinates all the downstream steps of miRNA-mediated repression events (Eulalio et al., 2009). First, it binds to poly(A) binding protein (PBP) on the poly(A) tail of the mRNA and stops translation initiation, after which it recruits the deadenylase CCR4-NOT and the decapping DCP1-DCP2 complexes (Behm-Ansmant et al., 2006; Chekulaeva et al., 2011; Zekri et al., 2009). The CCR4-NOT1 also recruits the translational repressor DDX6 (Mathys et al., 2014). Following deadenylation, the shortened poly(A) tail triggers the DCP1/DCP2 decapping complex to remove the 5′ cap of the mRNA, leading to degradation by the 5′ to 3′ exoribonuclease Xrn1. GW182 thus mediates translational inhibition at early stages followed by mRNA decay (Bazzini et al., 2012; Bethune et al., 2012; Chen et al., 2014).

In mammals, there are 3 paralogs of GW182 called TNRC6 a, b and c, which are thought to be functionally redundant because each of the three can associate with all four Ago proteins and repress the bound target mRNA in tethering assays (Landthaler et al., 2008; Lazzaretti et al., 2009; Tritschler et al., 2010; Zipprich et al., 2009). Moreover, small interfering RNA (siRNA) silencing in cell lines of any of the three paralogs partially relieves miRNA-mediated target mRNA repression in luciferase reporter assays (Tritschler et al., 2010; Zipprich et al., 2009).

Author Manuscript Author Manuscript Author Manuscript Author Manuscript

To assess the in vivo function of TNRC6 family members, we generated TNRC6a, TNRC6b, and TNRC6c knockout mice. Deletion of TNRC6a results in embryonic lethality, whereas a majority of TNRC6b and all TNRC6c null mutants die within one day after birth, the latter with signs of respiratory failure. TNRC6c mutant lungs at birth demonstrate thick-walled gas exchange saccules lined by mature alveolar epithelial type 1 (AT1) and AT2 cells but surrounded by an immature microvasculature. These structural defects are associated with a dynamic reduction in Transforming Growth Factor beta (TGFβ) genes, well-established drivers of sacculation.

2. Materials and methods

2.1. Mice and animal care

TNRC6a, b and c heterozygous null mice were generated at the Texas A&M Institute for Genomic Medicine (TIGM) using C57BL/6 gene trap embryonic stem (ES) cell clones IST12137A2 (TNRC6a), IST12075C8 (TNRC6b), and IST11346C2 (TNRC6c). Details of gene trap insertion can be found at the Jackson Laboratory database (http//www.informatics.jax.org/allele/key/268085 for TNRC6a; /allele/key/257627 for TNRC6b; and /allele/key/217717 for TNRC6c). Heterozygotes were crossed at Texas Tech University Health Science Center (TTUHSC) and pups genotyped by PCR using tail snips at 2 weeks of age (primer sequences in Supplementary Table 1). For timed pregnancy, noon on the day of discovery of the vaginal plug was considered as embryonic day 0.5 (E0.5). All animal studies were approved by the TTUHSC Institutional Animal Care and Use Committee.

2.2. Histology and electron microscopy

The offspring of TNRC6c heterozygous intercrosses were euthanized by decapitation, fixed in Bouin's solution (Cat. HT10132, Sigma-Aldrich) at 4 °C for 16–24 h, transferred into 70% ethanol, then submitted to the whole mouse phenotyping service at Yale University School of Medicine. Isolated lungs from embryonic and postnatal stages were also collected for staining with Hematoxylin and Eosin (H & E) as described below. For scanning electron microscopy, lungs from newborn pups were removed en block from the thorax, manually sliced, then fixed in 4% glutaraldehyde with 0.05 M cacodylate buffer at pH of 7 overnight at 4 °C. Lungs were then briefly rinsed twice in cacodylate buffer, incubated for two hours in buffered osmium tetroxide at 4 °C, then transferred through a graded series of ethanol up to 100% anhydrous ethanol. Prior to imaging, specimens underwent critical point drying, mounting, and sputter coating with 60% gold and 40% palladium. Images were collected on the Hitachi S-4300 high resolution field emission SEM1.

2.3. Lung immunofluorescence staining and microscopy

Lungs were isolated from mice decapitated at the stages indicated and individual lobes immersion-fixed in 4% paraformaldehyde (PFA) overnight at 4 °C with gentle rocking, submerged in OCT (Tissue Tek) in embedding molds, frozen on dry ice, then stored at −80 °C. Alternatively, some lobes were manually sliced into approximately 4 × 4 mm pieces which were immersion-fixed in Dent's solution over-night at 4°C with gentle rocking, transferred to 100% methanol, then stored at −20 °C. For staining of cryopreserved lungs, 14 μm sections were cut using a cryostat (Leica CM3050S) and collected on Superfrost

Author Manuscript Author Manuscript Author Manuscript Author Manuscript

Plus glass slides (Fisher Scientific) then allowed to air dry. Similar protocols were used for immunostaining of sections and whole mount lung tissue, but with increased incubation times for whole mounts. For whole mount staining, specimens were sequentially rehydrated in 75%, 50%, and 25% methanol in PBS + 0.1% Tween-20 (PBS-T), then washed in PBS-T for 10 min at room temperature (RT). Cryosectioned tissue underwent antigen retrieval by boiling slides for 7 min at 100 °C in Citrate buffer (10 mM Citric Acid, 0.05% Tween 20, pH 6). Slides were cooled down to RT then rinsed in PBS-T for 2 min at RT × 2. Specimens were incubated in blocking solution (PBS + 10% goat serum, 3% bovine serum albumin, and 0.1% Triton-X-100) for one hour at RT × 2, then with primary antibodies in block solution overnight at 4 °C. Primary antibodies (used at 1:500 unless otherwise specified) were against the following antigens: Acetylated tubulin (Acet tub, mouse, Sigma T6793; clone 6-11B-1), Podoplanin (Pdpn, hamster, DSHB 8.1.1, 1:20 dilution), Secretoglobin 1a1 (Scgb1a1, rabbit, Upstate), pro-surfactant protein C (pSftpc, rabbit, Millipore), Cleaved Caspase-3 (Casp3, Alexa 488-conjugated, rabbit, R & D systems), NK2 Homeobox 1 (Nkx2.1, biotinylated, mouse, Abcam, clone 8G7G3/1), ETS related gene (ERG, rabbit, Abcam, clone EPR3864), Marker of Proliferation Ki-67 (MKi67, biotinylated, rat, eBioscience, clone SolA15), and Endomucin (Emcn, goat, R & D systems). Following primary antibody incubation, specimens were washed in block solution for one hour at RT × 2 (slides) or at RT × 5 at 4 °C (whole mounts), then incubated with secondary antibodies (1:250) +/− streptavidin (1:250) and DAPI (5 ng/mL) in block solution for one hour (slides) or overnight (whole mounts) at 4 °C. Goat secondary antibodies and streptavidin were conjugated to Alexa fluorophores (A488, A555, A633; Invitrogen). Specimens were then washed in PBS for 2 min (slides) or 30 min (whole mounts) at RT × 5, mounted in Vectashield (Vector) and coverslipped (slides) or immersed in 80% glycerol (whole mounts), then stored at 4 °C until imaging. For imaging of whole mounts, specimens were transferred into chambered coverslips (Falcon) and submerged in Vectashield. Immunostained lungs were analyzed and images acquired using an inverted laser scanning confocal microscope (Leica Sp8) with LCS software, then processed (pseudocolored, levels and contrast adjusted) using Adobe Photoshop (CS5.1).

2.4. Western blotting

E18.5 or P0 lungs were homogenized in RIPA lysis buffer containing Protease Inhibitor Cocktail (Roche Product No. 11836153001) and 1 mM PMSF. Lysates were centrifuged at 4000 × *g* for 10 min at 4 °C, and the resulting supernatants were analyzed by immunoblotting. Protein quantification was performed with the BCA method (Pierce). Proteins were blotted on PVDF membranes and stained using antibodies against pro-SPB (NB600-1115, Novus Biologicals), AQP5 (PA1230, Boster Biological Technology), PCNA (sc-25280, Santa Cruz Biotechnology), Flk-1 (sc-505, Santa Cruz Biotechnology), Nkx2.1 (NB100-80062, Novus Biologicals), and Actb (Catalog #3700, Cell Signaling) at 1:1000 – 1:5000 dilutions. The Western blot quantification was performed with ImageQuantTL.

2.5. Quantification of cells

Lungs co-stained for combinations of nuclear markers (ERG-endothelial; Nkx2.1- epithelial; Casp3- apoptotic; MKi67- proliferating; DAPI- all cells) were quantified manually (MKi-67, Casp3) and automatically using CellProfiler (ERG, Nkx2.1, DAPI) in a blinded fashion in randomly selected alveolar fields (Carpenter et al., 2006). The customized CellProfiler

Author Manuscript Author Manuscript Author Manuscript Author Manuscript

pipeline was as follows: "Enhance or Suppress" (Suppress for nuclei) and "Identify Primary Objects" (diameter range 10–26 pixels) with Automatic Thresholding (Otsu method) and Method to distinguish clumped objects (Laplacian of Gaussian, Propagate method to draw diving lines between clumped objects). The results of automated quantification were confirmed by manual verification of scored field for quality control.

2.6. Quantification of Mesenchyme thickness

Lungs were isolated and fixed in 4% PFA for 16–24 h at 4 °C, then paraffin-embedded using standard procedures. Using a microtome, 6 μm sections from the same regions of lungs oriented in the same positions from each animal were collected on glass slides, deparaffinized, rehydrated, and processed for routine H & E staining. Lungs were imaged at 40× magnification using a Nikon compound microscope equipped with a digital color camera. For each of the wild type and TNRC6c knockout animals at each reported age, images from four randomly selected alveolar fields were captured and exported as RGB TIF files for analysis using MATLAB's image processing toolbox (MathWorks®). In a blinded manner, air sacs were thresholded using Otsu's method (Sezgin and Sankur, 2004) and inverted to represent the mesenchymal cells as a binary mask. To calculate the thickness of the mesenchyme, the pixels occupied by the binary mask within random alveolar fields were summed.

2.7. Quantification of pulmonary gas exchange interface and microvascular maturation

Whole mount lung specimens at indicated ages were stained as described above to mark the epithelial surface (Pdpn, AT1 cells) and vasculature (endothelial "cocktail"). Endothelial "cocktail" included antibodies against Platelet/endothelial cell adhesion molecule 1 (PECAM1/CD31, rat, BD Pharmingen) and MECA32 (rat, DSHB). Images were then obtained as stacks of approximately 40 μm in the z dimension, beginning with the immediate sub-mesothelial region and proceeding internally. For assessment of pulmonary gas exchange interface, the epithelial (AT1) and vasculature images were thresholded separately using Otsu's method as described above. Element-wise multiplication was used to identify the pixels that were common to both images, i.e. the areas where the two images colocalized. For quantification, the number of colocalized pixels were summed and divided by the area of the field of view. For determination of microvascular density, maximum intensity projections (MIP), each made up of five consecutive optical slices, were calculated for each stack. The intensity values of each pixel of an MIP were summed and divided by the total area of the image. All analyses were performed in a blinded manner.

2.8. Quantitative reverse transcription polymerase chain reaction (qRT-PCR)

Total RNA was isolated from mouse lung tissue at E17.5 and E18.5 using the RNAeasy kit (Qiagen) and treated with DNase1 (Qiagen) according to the manufacturer's instructions. Isolated RNA was reverse-transcribed using SuperScript III first-strand Synthesis SuperMix (Catalog #18080-400, Life Technologies) according to the manufacturer's protocols. SYBR® Green PCR Master Mix (Applied Biosystems) and commercially available TaqMan gene expression assays (Applied Biosystems) were used for qRT-PCR analyses. Expression levels were normalized to that of beta actin or glyceraldehyde-3-phosphate dehydrogenase (Gapdh). Primer sets used in the study are reported in Supplementary Table 1.

Author Manuscript Author Manuscript Author Manuscript Author Manuscript

2.9. Statistics

Statistical analyses were performed using GraphPad software. The graphs are expressed as mean ± 1 standard deviation (SD). p-values were calculated using Student's *t*-test with $p \leq 0.05$ considered statistically significant. P-values reporting statistical significance of quantitative image analyses were calculated with the Wilcoxon Rank Sum test.

3. Results

3.1. Confirmation of paralog-specific, germline deletion of TNRC6a, b and c

To confirm the specificity of paralog-specific TNRC6 deletions, we used qRT-PCR to measure transcript levels of each of the three paralogs in each of the different null mutants. TNRC6c null mutants expressed similar levels of TNRC6a and b as wild type (WT) mice, whereas TNRC6c was undetectable (> 35 fold lower than WT) (Fig. 1a). Similar results confirmed paralog-specific deletion in TRC6a and b null mice (data not shown). We were unable to further confirm deletion at the protein level because paralog-specific antibodies against TNRC6 are not available. However, the fact that each of the mutants demonstrated a phenotype supports that each paralog was successfully targeted.

3.2. TNRC6a, b and c knockout mice display distinct patterns of lethality

Heterozygous TNRC6 mice were mated and pups initially genotyped two weeks after birth. At this age, TNRC6b null mutants were detected at less than Mendelian ratio (12/161, 7.5%) but no homozygous null TNRC6a or TNRC6c pups were identified (Supplementary Table 2). The surviving TNRC6b null mice displayed significantly reduced body size during the first months of life and were apparently infertile because no offspring could be derived by mating them with wild type or heterozygous 6b mutant mice.

To determine the time of lethality in the TNRC6a and c null mice, offspring were genotyped at postnatal day 0 (PN0). For TNRC6a, no homozygous mutants were detected at birth, indicating embryonic lethality. We therefore collected embryos at progressive gestational ages and found that although TNRC6a null embryos could be detected at E 9.5 (n = 8 dams), none were found at E12.5 (n = 3 dams). This observation is consistent with a recent report from Jiang et. al. that TNRC6a knock out embryos die at E12.5 due to defects in the yolk sac endoderm (Jiang et al., 2012).

For TNRC6c, homozygotes were born at a Mendelian frequency (42/182, 23%), but a subset (~12%) developed cyanosis and a rapid respiratory rate shortly after birth (Fig. 1b & Supplementary Video 1) and typically died within the first 6 h. The remaining TNRC6c mutants progressively died over the next 18 h (Fig. 1c). TNRC6b mutants that died as neonates and ones that survived to adulthood, by contrast, did not exhibit cyanosis or signs of respiratory distress.

Supplementary material related to this article can be found online at http://dx.doi.org/10.1016/j.ydbio.2017.07.018.

Author Manuscript Author Manuscript Author Manuscript Author Manuscript

3.3. Organogenesis defects in TNRC6c null mice are restricted to the gas exchange region of the lungs

TNRC6c null pups were comparable to WT siblings in body weight and developmental stage and had normal hematocrit suggesting no defects in erythropoiesis (not shown). In order to determine the cause of death, H & E stains of PN0 embryos were generated and all organs examined in a blinded manner by a veterinary pathologist. Except for the lungs, organs in TNRC6c null pups appeared histologically normal and were indistinguishable from the corresponding organs in WT pups (Fig. 1d). Mutant lungs, by contrast, demonstrated normal-appearing airways terminating in small distal gas exchange sacs separated by inappropriately thick mesenchyme, although the severity of this phenotype was variable (Fig. 1d–e, Supplementary Fig. 1). In conjunction with the clinical observation of cyanosis and respiratory distress, these findings suggest that the lethality from TNRC6c deletion resulted from respiratory failure due to defective morphogenesis of the gas exchange region of lung, as examined below.

3.4. Lung epithelial cell differentiation is not disrupted by deletion of TNRC6c

Pulmonary gas exchange takes place in distal alveolar sacs lined by two epithelial cell types that differentiate from a bipotent progenitor shortly before birth (Desai et al., 2014; Treutlein et al., 2014). Incredibly thin alveolar epithelial type (AT) 1 cells facilitate passive diffusion of oxygen and carbon dioxide between the airspace lumen and underlying microvasculature, while cuboidal AT2 cells secrete surfactant phospholipid into the airspace that minimizes surface tension to prevent alveolar collapse (Morrisey and Hogan, 2010). Functional AT1 and AT2 cells are required for proper gas exchange after birth, as evidenced by respiratory insufficiency in newborn infants with neonatal Interstitial Lung Disease or extreme prematurity (Kuo and Desai, 2015). To assess for the presence and distribution of differentiated lung epithelial cell types, we co-stained E18.5 and PN0 TNRC6c null and WT lungs for AT1, AT2, ciliated, and Club cell type markers. The stains revealed that each of these cell types was present and properly localized within the mutant lungs, in a similar pattern as in WT siblings. Conducting airways were lined by ciliated (acetylated tubulin) and Club (Secretoglobin 1a1, Scgb1a1) cells, while gas exchange sacs were populated by cuboidal AT2 (Surfactant protein C, Sftpc) and flat AT1 (Podoplanin, Pdpn) cells (Fig. 2a–b). While the level of expression of Sftpc was slightly reduced in TNRC6c mutant lungs at PN0, cuboidal AT2 cells interspersed with flat AT1 cells were present at E18.5. Given this result, and the fact that most mutants did not experience rapid respiratory distress or cyanosis at birth, functional AT2 cells were presumably present and produced sufficient surfactant phospholipid to preclude acute respiratory distress syndrome. We also measured protein levels of Aquaporin 5 (Aqp5, AT1) and Surfactant protein B (Sftpb, AT2), important functional markers of mature AT1 and AT2 cells that are not expressed by embryonic progenitors (Desai et al., 2014). Both proteins were expressed by mutants at levels comparable to WT littermates by E18.5 (Fig. 2C). Therefore, the eventual respiratory failure in TNRC6c mutant pups over 24 h after birth is not likely attributable to an absence or dysfunction of mature lung epithelial cells, and suggests an alternate etiology for the progressive cyanosis and increased work of breathing.

Author Manuscript Author Manuscript Author Manuscript Author Manuscript

3.5. Loss of TNRC6c impairs mesenchymal thinning during airspace sacculation without altering cellular kinetics or composition in the distal lung

Lung morphogenesis in mice begins with the early pseudoglandular stage (E9.5–16.5) followed by the canalicular (E16.5– 17.5), then the terminal saccular (E17.5-PN5) stages (Warburton et al., 2010). To more precisely characterize the phenotype of TNRC6c null mice, we examined the lungs at E16.5, E17.5 and E18.5. No gross or histological abnormalities were identified at E16.5 and E17.5, suggesting that the phenotype observed at birth resulted from defective sacculation. Sacculation involves the co-ordinated morphogenesis of surfactant-producing AT2 cells and flat AT1 cells with concomitant dilation of the terminal airway lumen, thinning of surrounding mesenchyme, and remodeling of the capillary network. This dynamic process culminates in a densely packed collection of thin-walled distal air sacs, tightly apposed to an underlying capillary mesh, that are capable of efficient gas exchange upon birth (Burri and Moschopulos, 1992). TNRC6c null lungs at E18.5 and PN0 demonstrate an inappropriately thick mesenchyme and small air sacs seen in cross-section by H & E staining (Fig. 3a), while immunohistochemistry for NK2 Homeobox 1 (Nkx2.1) marking lung epithelial cell nuclei showed a normal pattern of admixture with non-epithelial cells (Fig. 3b). Distal lung was also directly visualized in three dimensions by scanning electron microscopy, which clearly demonstrated thick mesenchymal walls separating air sacs in mutant compared with WT lungs at birth (Fig. 3c). Quantification confirmed significantly thicker air sac mesenchyme in null mutants at E18.5, and while some thinning was evident at PN0, it remained significantly thicker than in WT littermates at birth (Fig. 3d). Quantitation also confirmed no difference in epithelial cell proportions between mutant and WT distal lungs at E18.5 and PN0 (Fig. 3e), and apoptosis and proliferation rates were low but also comparable at these stages (Fig. 3f–h). Overall, this phenotype indicates a failure to complete the process of sacculation in TNRC6c null mutant lungs. The lack of a significant difference in cellular kinetics and epithelial cell proportion suggests that the thickened mesenchyme results from a defect in dynamic structural remodeling, rather than from an excess of cells.

3.6. Defective formation of the distal gas exchange interface and impaired microvascular maturation in TNRC6c null mutants

Despite the presence of functional AT1 and AT2 cells at birth, TNRC6c mutants develop cyanosis with tachypnea and progressive respiratory failure over the first postnatal day. Proper gas exchange at birth requires not only mature alveolar epithelial cells, but also establishment of a minimal barrier for passive gas diffusion (Meban, 1980). Therefore, it is essential that remodeling of the microvasculature that culminates in tight apposition of underlying capillaries to ultra-thin AT1 cells occurs in parallel with cellular differentiation. This process is driven by production of Vascular Endothelial Growth Factor A (VEGF-A) by newly-maturing AT1 cells that signals to underlying endothelial cells expressing the VEGFR2 (Kdr), inducing their proliferation and migration towards the epithelial surface (Yamamoto et al., 2007). To assess this functional gas exchange interface, we performed combinatorial immunostaining of the lungs for AT1 and endothelial cell markers at PN0. The results showed tight apposition of endothelial and epithelial cells in primitive gas exchange sacs and a dense capillary mesh in WT lungs. By contrast, the expected close physical association of endothelial and epithelial cells was lacking (Fig. 4a–b) and the

Author Manuscript Author Manuscript Author Manuscript Author Manuscript

capillary network was significantly more rudimentary and less dense (Fig. 4c–d) in mutant lungs, resembling the pre-sacculation vascular plexus. These results suggest that the normal interactions between nascent AT1 and capillary endothelial cells that drive their migration and proliferation, as well as maturation of the capillary mesh, were disrupted in TNRC6c mutants (Hines and Sun, 2014). The inappropriately long distance between the airspace and microvasculature across which gas must diffuse also provides an explanation for the increased work of breathing and cyanosis observed in mutant pups despite the presence of functional AT1 and AT2 cells. We also assessed endothelial cell number in the distal lung by staining for ERG, a marker of endothelial cell nuclei (Fig. 4e). Quantification showed no difference in the proportion of endothelial cells between WT and mutant lungs at either E18.5 or PN0 (Fig. 4f). Together, these findings suggest that the observed defect in microvascular maturation in TNRC6c null mutant lungs results from impaired dynamic structural remodeling of the vascular plexus, rather than from an insufficient number of endothelial cells.

3.7. TGFβ and VEGF family genes are dynamically reduced in TNRC6c mutant lungs during sacculation

TGFβ family genes are expressed (Zhao and Young, 1995; Chen et al., 2008) and signaling is active in the distal lung throughout the process of sacculation (Alejandre-Alcazar et al., 2008). TGFβ signaling is essential for proper thinning of the mesenchyme during this process, with genetic deletion of various pathway members resulting in thick-walled air sacs and neonatal death (Bjork et al., 2010; Kaartinen et al., 1995; Shi et al., 1999), resembling the TNRC6c mutant phenotype. Concomitant with mesenchyme thinning and airspace expansion, newly-maturing AT1 cells initiate expression of VEGF-A that attracts underlying endothelial cells expressing VEGFR2, which induces their proliferation and apposition to the epithelial surface (Yamamoto et al., 2007; Hines and Sun, 2014). To determine if disruption of TGFβ and/ or VEGF signaling was involved in the TNRC6c mutant phenotype, we measured the lung expression of TGFβ and VEGF family members at E17.5 and E18.5 by qRT-PCR. We found normal levels at E17.5, but a significant reduction in mutant lungs of both TGFβ1 and TGFβR2 at E18.5 (Fig. 4g). VEGF-A was not reduced at either stage, while VEGFR1 (Flt1) and VEGFR2 (Kdr) were significantly lower at E18.5 compared to WT littermates. Kdr protein was also reduced in mutant lungs by 60% compared with WT levels at E18.5 (Fig. 4h). The results suggest that TGFβ signaling activity is dynamically reduced during sacculation in TNRC6c mutants at the time when it is essential for proper mesenchyme thinning. Whether the reduction in VEGFR1 and 2 at E18.5 was a cause of the microvascular defect (by reducing signaling activity) or merely reflected the lower capillary density is uncertain, but given the proper expression of VEGF-A ligand and normal proportion of endothelial cells, we favor the latter model.

4. Discussion

The three paralogs of GW182 are generally thought to be functionally redundant because TNRC6a, b and c proteins can each associate with all four Ago proteins and repress the bound target mRNA in tethering assays (Landthaler et al., 2008; Lazzaretti et al., 2009; Tritschler et al., 2010; Zipprich et al., 2009). Moreover, siRNA silencing of TNRC6a, b or

Author Manuscript Author Manuscript Author Manuscript Author Manuscript

c in cell lines each partially relieve miRNA-mediated target mRNA repression in luciferase reporter assays, suggesting they have equivalent actions (Tritschler et al., 2010; Zipprich et al., 2009). However, as our results show, each paralog has a distinct role in vivo. Several possibilities could explain this apparent contradiction. One is that each paralog may in fact exert different actions. Because only a few out of hundreds of miRNA targets have been tested in tethering assays and RNAi silencing experiments, paralog-specific miRNA/target mRNA pairs may exist that have not yet been identified. Indeed, in TNRC6a knockout mice (which are embryonic lethal due to defects in the yolk sac endoderm), although TNRC6b and c are also both expressed in the endoderm, there is selective de-repression of the targets of miR-17/20/93/106 clusters (Jiang et al., 2012), suggesting that TNRC6a may be specific for these targets. Another possible explanation for the distinct phenotypes is that the paralogs may be differentially expressed in the developing embryo. Although expression analysis of human and mouse tissues and cell lines suggest that TNRC6a, b and c, are each ubiquitously expressed (Ramskold et al., 2009), these studies were performed on bulk cells, which could mask differences in expression at the level of individual cells. It has also been recently shown that TNRC6 family members possess nuclear localization and nuclear export signals, so shuttling between cytoplasm and nucleus may influence gene transcription (Schraivogel et al., 2015). This effect and/or differential trafficking leading to variability in the cytoplasmic levels of TNRC6 proteins could yield different gene expression patterns between cells that express the same paralogs (Matsui et al., 2013).

Although the severity and timing of onset of respiratory distress varied considerably (obvious cyanosis and tachypnea was immediately apparent in ~12% of pups), all TNRC6c mutants died within 24 h after birth. This variability in respiratory insufficiency was correlated with differences in the severity of the observed lung phenotype between individual mutants (Supplemental Fig. 1). The reason for this variation is not apparent, although it is possible that differences in regulative induction of one or both of the other paralogs between individual animals might partially compensate for the absence of TNRC6c. Another possibility is that alternative splicing resulted in variable, low level expression of TNRC6c protein, which has been reported in up to 10% of mutants generated using gene trap approaches (Guan et al., 2010). Unfortunately, we could not assess for this possibility because of the unavailability of paralog-specific antibodies.

The lung phenotype in TNRC6c null mice appears to result from incomplete sacculation, with varying degrees of mesenchyme thinning, endothelial-AT1 cell apposition, and microvascular maturation observed between individual mutants. Gene-targeted mice deficient for TGFβ signaling demonstrate a similar structural phenotype and die within the first day of birth, but typically also manifest with a cleft secondary palate (Bjork et al., 2010; Kaartinen et al., 1995; Shi et al., 1999). TGFβ mutants have not to our knowledge been investigated for endothelial cell apposition and microvascular maturation defects, perhaps because their mortality is presumed to result from starvation due to the inability to suckle. Future studies in TGFβ pathway and other mutants with thickened mesenchyme, in which the VEGF pathway is not targeted, will be useful for determining whether the apposition and microvascular maturation defects in TNRC6c mutants are indirect consequences of a thickened mesenchyme. We cannot tease apart whether there is a causal relation between the failure of mesenchyme thinning and lack of microvascular remodeling, since we do

Author Manuscript Author Manuscript Author Manuscript Author Manuscript

not know whether the reduced VEGFR2 causes or merely reflects the simplified capillary network. Another group has previously reported that attenuated VEGF signaling (from germline deletion of two of the three isoforms) resulted in impaired microvascular and delayed airspace maturation (Galambos et al., 2002). This raises the possibility that microvascular phenotype could be the primary defect and indirectly disrupt the process of mesenchyme thinning. Interestingly, genetic overexpression of VEGF-A in distal mouse lung in the perinatal period was reported to increase endothelial cell numbers but also inhibited mesenchymal thinning, supporting an interdependence of microvascular maturation and mesenchymal thinning (Mallory et al., 2006). The significance of the reduced level of expression of Sftpc by AT2 cells in mutants at PN0, but not E18.5, is also uncertain. Previous studies have also reported that Sftpc expression (Kaartinen et al., 1995) and/or the number of AT2 cells (Shi et al., 1999) is reduced at birth in conjunction with the thickened air sacs in TGFβ pathway mutants, although in TNRC6c mutants there doesn't appear to be an effect on cell numbers. In any case, as mentioned above, the absence of acute respiratory distress in the vast majority of newborn mutant pups and similar expression levels of Sftpb protein strongly suggest that the AT2 cells are producing functional surfactant.

In terms of the significance of reduced TGFβ1 and TGFβR2, it has been previously reported that deletion of TGFβ1 generates systemic inflammation, including in the lungs, but sacculation was unaffected (Shull et al., 1992; Kulkarni et al., 1993). TGFβR2 has also been studied, and its conditional deletion in the developing lung epithelium does not disrupt air sac morphogenesis, although interestingly due to an apparent defect in secondary septation that occurs postnatally, alveoli actually become pathologically enlarged (Chen et al., 2008; Li et al., 2011). TGFβR2 is also normally expressed by distal lung mesenchyme throughout the process of sacculation, but its role in this process remains unknown because conditional deletion of TGFβR2 in developing lung mesenchyme is lethal by E16.5 (Chen et al., 2008; Li et al., 2008).

Regarding the mechanism by which TGFβ expression is altered, although as mentioned, TNRC6 proteins may play a nuclear role in regulating transcription, only one such example exists (Matsui et al., 2013). We therefore suggest that the observed defect is more likely mediated by dysregulation of miRNA effector function. Because the absence of TNRC6c should result in failure to repress an mRNA, the downregulation of TGFβ1 and the receptor, TGFβR2, is presumably an indirect effect, for example by the failure of miRNA-mediated repression of one or more genes that inhibit TGFβ expression. Further work will be needed to identify the putative intermediate effector and elucidate the exact mechanism by which TNRC6c induces TGFβ1 and TGFβR2, as well as to determine if it directly regulates VEGFR expression in lung endothelial cells. As we stated earlier, we favor that the reduced VEGFR2 merely reflects the lowered surface area of endothelial cells in the immature plexus, since the proportion of endothelial cells is not reduced. If so, this would suggest that the microvascular immaturity is a consequence, rather than a cause, of the inappropriately thick mesenchyme. However, as we noted above, genetic targeting of VEGF isoforms was reported to produce inappropriately thick mesenchyme, which implies that microvasculature maturation promotes mesenchymal thinning. Thus, it seems plausible that dynamic bi-directional signaling between tissue layers is essential for navigating sacculation

Author Manuscript Author Manuscript Author Manuscript Author Manuscript

in a manner that culminates in a highly stereotyped collection of functional gas exchange sacs.

In summary, TNRC6 paralogs have distinct functions in vivo and TNRC6c appears to be selectively required for several aspects of sacculation, namely, mesenchymal thinning, establishing AT1-endothelial cell apposition, and maturation of the capillary mesh. These processes are mediated at least in part by TNRC6c promoting expression of TGFβ family genes that are well known mediators of mesenchymal thinning. Our findings show that TNRC6c plays an essential role in airway sacculation that is upstream of TGFβ, and suggest that it normally acts indirectly by effecting degradation of one or more mRNAs that encode an inhibitor of TGFβ1 and TGFβR2 expression. Identifying these putative mRNAs will be a high priority, since they could be involved in the pathogenesis of neonatal lung diseases in which both alveolar mesenchyme and microvasculature is disrupted, like bronchopulmonary dysplasia, or be harnessed for promoting repair of the gas exchange interface following injury in adult life (Logan and Desai, 2015).

Supplementary Material

Refer to Web version on PubMed Central for supplementary material.

Acknowledgments

We thank Andres Andalon for technical assistance, and Astrid Gillich and Anne Hilgendorff for valuable discussions.

Funding

This work was supported by Howard Hughes Medical Institute Gilliam Fellowship (F.E.O.), Stanford Graduate Fellowship (F.E.O.), NHLBI 1R56HL12747101 (T.J.D.), and NIAID U19 AI 056900 (M.S). T.J.D. is a Stanford Child Health Research Institute 2016 Faculty Scholar.

References

Alejandre-Alcazar MA, et al. 2008; TGF-beta signaling is dynamically regulated during the alveolarization of rodent and human lungs. Dev. Dyn. 237 :259–269. [PubMed: 18095342]

Baillat D, Shiekhattar R. 2009; Functional dissection of the human TNRC6 (GW182-related) family of proteins. Mol. Cell. Biol. 29 :4144–4155. [PubMed: 19470757]

Bartel DP. 2004; MicroRNAs: genomics, biogenesis, mechanism, and function. Cell. 116 :281–297. [PubMed: 14744438]

Bazzini AA, Lee MT, Giraldez AJ. 2012; Ribosome profiling shows that miR-430 reduces translation before causing mRNA decay in zebrafish. Science. 336 :233–237. [PubMed: 22422859]

Behm-Ansmant I, et al. 2006; mRNA degradation by miRNAs and GW182 requires both CCR4:NOT deadenylase and DCP1:DCP2 decapping complexes. Genes Dev. 20 :1885–1898. [PubMed: 16815998]

Bethune J, Artus-Revel CG, Filipowicz W. 2012; Kinetic analysis reveals successive steps leading to miRNA-mediated silencing in mammalian cells. EMBO Rep. 13 :716–723. [PubMed: 22677978]

Bjork BC, Turbe-Doan A, Prysak M, Herron BJ, Beier DR. 2010; Prdm16 is required for normal palatogenesis in mice. Hum. Mol. Genet. 19 :774–789. [PubMed: 20007998]

Burri PH, Moschopulos M. 1992; Structural analysis of fetal rat lung development. Anat. Rec. 234 :399–418. [PubMed: 1443666]

Carpenter AE, et al. 2006; CellProfiler: image analysis software for identifying and quantifying cell phenotypes. Genome Biol. 7 :R100. [PubMed: 17076895]

Author Manuscript Author Manuscript Author Manuscript Author Manuscript

Carthew RW, Sontheimer EJ. 2009; Origins and mechanisms of miRNAs and siRNAs. Cell. 136 :642–655. [PubMed: 19239886]

Chekulaeva M, et al. 2011; miRNA repression involves GW182-mediated recruitment of CCR4-NOT through conserved W-containing motifs. Nat. Struct. Mol. Biol. 18 :1218–1226. [PubMed: 21984184]

Chen H, et al. 2008; TGF-beta receptor II in epithelia versus mesenchyme plays distinct roles in the developing lung. Eur. Respir. J. 32 :285–295. [PubMed: 18321928]

Chen Y, et al. 2014; A DDX6-CNOT1 complex and W-binding pockets in CNOT9 reveal direct links between miRNA target recognition and silencing. Mol. Cell. 54 :737–750. [PubMed: 24768540]

Desai TJ, Brownfield DG, Krasnow MA. 2014; Alveolar progenitor and stem cells in lung development, renewal and cancer. Nature. 507 :190–194. [PubMed: 24499815]

Doench JG, Sharp PA. 2004; Specificity of microRNA target selection in translational repression. Genes Dev. 18 :504–511. [PubMed: 15014042]

Dueck A, Meister G. 2014; Assembly and function of small RNA - argonaute protein complexes. Biol. Chem. 395 :611–629. [PubMed: 24603840]

Eulalio A, Huntzinger E, Izaurralde E. 2008; GW182 interaction with Argonaute is essential for miRNA-mediated translational repression and mRNA decay. Nat. Struct. Mol. Biol. 15 :346–353. [PubMed: 18345015]

Eulalio A, Helms S, Fritzsch C, Fauser M, Izaurralde E. 2009; A C-terminal silencing domain in GW182 is essential for miRNA function. RNA. 15 :1067–1077. [PubMed: 19383769]

Galambos C, et al. 2002; Defective pulmonary development in the absence of heparin-binding vascular endothelial growth factor isoforms. Am. J. Respir. Cell Mol. Biol. 27 :194–203. [PubMed: 12151311]

Guan C, Ye C, Yang X, Gao J. 2010; A review of current large-scale mouse knockout efforts. Genesis. 48 :73–85. [PubMed: 20095055]

Hines EA, Sun X. 2014; Tissue crosstalk in lung development. J. Cell Biochem. 115 :1469–1477. [PubMed: 24644090]

Jiang Z, et al. 2012; Trinucleotide repeat containing 6a (Tnrc6a)-mediated microRNA function is required for development of yolk sac endoderm. J. Biol. Chem. 287 :5979–5987. [PubMed: 22187428]

Kaartinen V, et al. 1995; Abnormal lung development and cleft palate in mice lacking TGF-beta 3 indicates defects of epithelial-mesenchymal interaction. Nat. Genet. 11 :415–421. [PubMed: 7493022]

Kawamata T, Tomari Y. 2010; Making RISC. Trends Biochem. Sci. 35 :368–376. [PubMed: 20395147]

Kulkarni AB, et al. 1993; Transforming growth factor beta 1 null mutation in mice causes excessive inflammatory response and early death. Proc. Natl. Acad. Sci. USA. 90 :770–774. [PubMed: 8421714]

Kuo CS, Desai TJ. 2015; Cellular mechanisms of alveolar pathology in childhood interstitial lung diseases: current insights from mouse genetics. Curr. Opin. Pediatr. 27 :341–347. [PubMed: 25888154]

Landthaler M, et al. 2008; Molecular characterization of human Argonaute-containing ribonucleoprotein complexes and their bound target mRNAs. RNA. 14 :2580–2596. [PubMed: 18978028]

Lazzaretti D, Tournier I, Izaurralde E. 2009; The C-terminal domains of human TNRC6A, TNRC6B, and TNRC6C silence bound transcripts independently of Argonaute proteins. RNA. 15 :1059–1066. [PubMed: 19383768]

Lewis BP, Shih IH, Jones-Rhoades MW, Bartel DP, Burge CB. 2003; Prediction of mammalian microRNA targets. Cell. 115 :787–798. [PubMed: 14697198]

Li M, et al. 2008; Mesodermal deletion of transforming growth factor-beta receptor II disrupts lung epithelial morphogenesis: cross-talk between TGF-beta and Sonic hedgehog pathways. J. Biol. Chem. 283 :36257–36264. [PubMed: 18990706]

Li M, et al. 2011; Epithelium-specific deletion of TGF-beta receptor type II protects mice from bleomycin-induced pulmonary fibrosis. J. Clin. Invest. 121 :277–287. [PubMed: 21135509]

Author Manuscript Author Manuscript Author Manuscript Author Manuscript

Lian SL, et al. 2009; The C-terminal half of human Ago2 binds to multiple GW-rich regions of GW182 and requires GW182 to mediate silencing. RNA. 15 :804–813. [PubMed: 19324964]

Logan CY, Desai TJ. 2015; Keeping it together: pulmonary alveoli are maintained by a hierarchy of cellular programs. Bioessays. 37 :1028–1037. [PubMed: 26201286]

Mallory BP, et al. 2006; Lymphangiogenesis in the developing lung promoted by VEGF-A. Microvasc. Res. 72 :62–73. [PubMed: 16806288]

Manjunath N, Wu H, Subramanya S, Shankar P. 2009; Lentiviral delivery of short hairpin RNAs. Adv. Drug Deliv. Rev. 61 :732–745. [PubMed: 19341774]

Mathys H, et al. 2014; Structural and biochemical insights to the role of the CCR4-NOT complex and DDX6 ATPase in microRNA repression. Mol. Cell. 54 :751–765. [PubMed: 24768538]

Matsui M, et al. 2013; Promoter RNA links transcriptional regulation of inflammatory pathway genes. Nucleic Acids Res. 41 :10086–10109. [PubMed: 23999091]

Meban C. 1980; Thickness of the air-blood barriers in vertebrate lungs. J. Anat. 131 :299–307. [PubMed: 7462096]

Morrisey EE, Hogan BL. 2010; Preparing for the first breath: genetic and cellular mechanisms in lung development. Dev. Cell. 18 :8–23. [PubMed: 20152174]

Murchison EP, Hannon GJ. 2004; miRNAs on the move: miRNA biogenesis and the RNAi machinery. Curr. Opin. Cell Biol. 16 :223–229. [PubMed: 15145345]

Ramskold D, Wang ET, Burge CB, Sandberg R. 2009; An abundance of ubiquitously expressed genes revealed by tissue transcriptome sequence data. PLoS Comput. Biol. 5 :e1000598. [PubMed: 20011106]

Schraivogel D, et al. 2015; Importin-beta facilitates nuclear import of human GW proteins and balances cytoplasmic gene silencing protein levels. Nucleic Acids Res. 43 :7447–7461. [PubMed: 26170235]

Sezgin M, Sankur B. 2004; Survey over imaging thresholding techniques and quantitative performance evaluation. J. Electron Imaging. 13 :146–168.

Shi W, et al. 1999; TGF-beta3-null mutation does not abrogate fetal lung maturation in vivo by glucocorticoids. Am. J. Physiol. 277 :L1205–1213. [PubMed: 10600892]

Shull MM, et al. 1992; Targeted disruption of the mouse transforming growth factor-beta 1 gene results in multifocal inflammatory disease. Nature. 359 :693–699. [PubMed: 1436033]

Takimoto K, Wakiyama M, Yokoyama S. 2009; Mammalian GW182 contains multiple Argonaute-binding sites and functions in microRNA-mediated translational repression. RNA. 15 :1078–1089. [PubMed: 19398495]

Treutlein B, et al. 2014; Reconstructing lineage hierarchies of the distal lung epithelium using single-cell RNA-seq. Nature. 509 :371–375. [PubMed: 24739965]

Tritschler F, Huntzinger E, Izaurralde E. 2010; Role of GW182 proteins and PABPC1 in the miRNA pathway: a sense of deja vu. Nat. Rev. Mol. Cell Biol. 11 :379–384. [PubMed: 20379206]

Warburton D, et al. 2010; Lung organogenesis. Curr. Top. Dev. Biol. 90 :73–158. [PubMed: 20691848]

Yamamoto Y, Shiraishi I, Dai P, Hamaoka K, Takamatsu T. 2007; Regulation of embryonic lung vascular development by vascular endothelial growth factor receptors, Flk-1 and Flt-1. Anat. Rec. 290 :958–973.

Zekri L, Huntzinger E, Heimstadt S, Izaurralde E. 2009; The silencing domain of GW182 interacts with PABPC1 to promote translational repression and degradation of microRNA targets and is required for target release. Mol. Cell. Biol. 29 :6220–6231. [PubMed: 19797087]

Zhao Y, Young SL. 1995; Expression of transforming growth factor-beta type II receptor in rat lung is regulated during development. Am. J. Physiol. 269 :L419–426. [PubMed: 7573476]

Zipprich JT, Bhattacharyya S, Mathys H, Filipowicz W. 2009; Importance of the C-terminal domain of the human GW182 protein TNRC6C for translational repression. RNA. 15 :781–793. [PubMed: 19304925]

Author Manuscript Author Manuscript Author Manuscript Author Manuscript

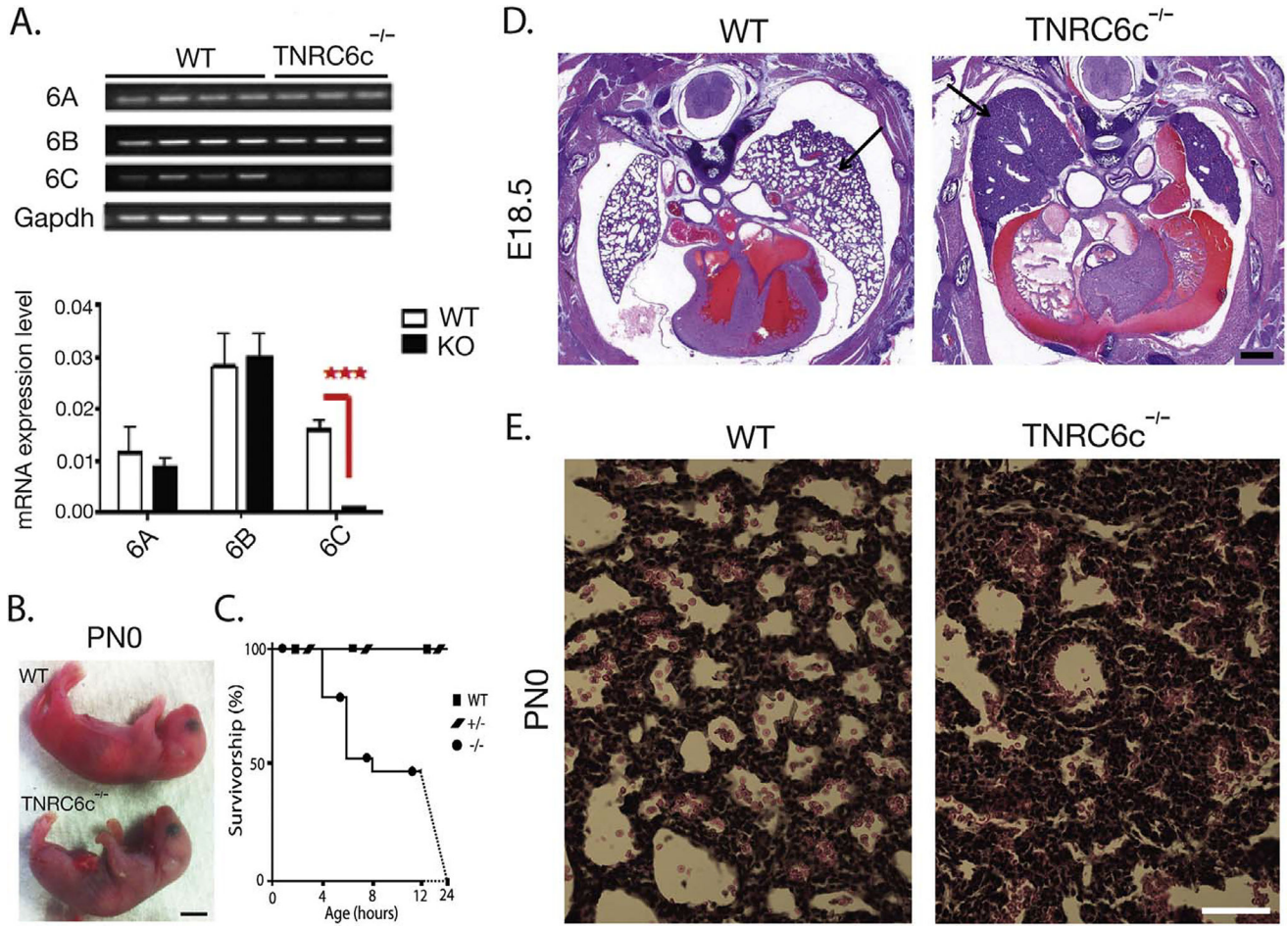

Fig. 1.

TNRC6c mutants develop cyanosis and die of respiratory failure within 24 h after birth. A. qRT-PCR for TNRC6a, b, c, and Gapdh in WT and TNRC6c null mutant mice. Representative gel picture shown above bar graph displaying cumulative results from n = 3–4 mice in each group. *** indicates $p < 0.001$. B. WT and TNRC6c null pups at PN0. Note cyanosis of null mutant. Scale bar, 4 mm. C. Survival curve showing WT (n = 22) and heterozygotes (n = 46) had no observed lethality, while TNRC6c null mutants (n = 20) all died within 24 h of birth. Dotted line indicates period over which specific time of death was not recorded. D. H & E of WT and TNRC6c null mice at E18.5 showing abnormal, dense appearance of lung tissue in mutant compared with WT (black arrows). Scale bar, 500 μm. E. H& E of WT and TNRC6c null mutant lungs at PN0 shows reduced air sac size and thickened mesenchyme in mutant. Scale bar, 50 μm. E, embryonic day; H & E, hematoxylin and eosin; KO, knockout; PN, postnatal day; WT, wild type.

Author Manuscript
Author Manuscript
Author Manuscript
Author Manuscript

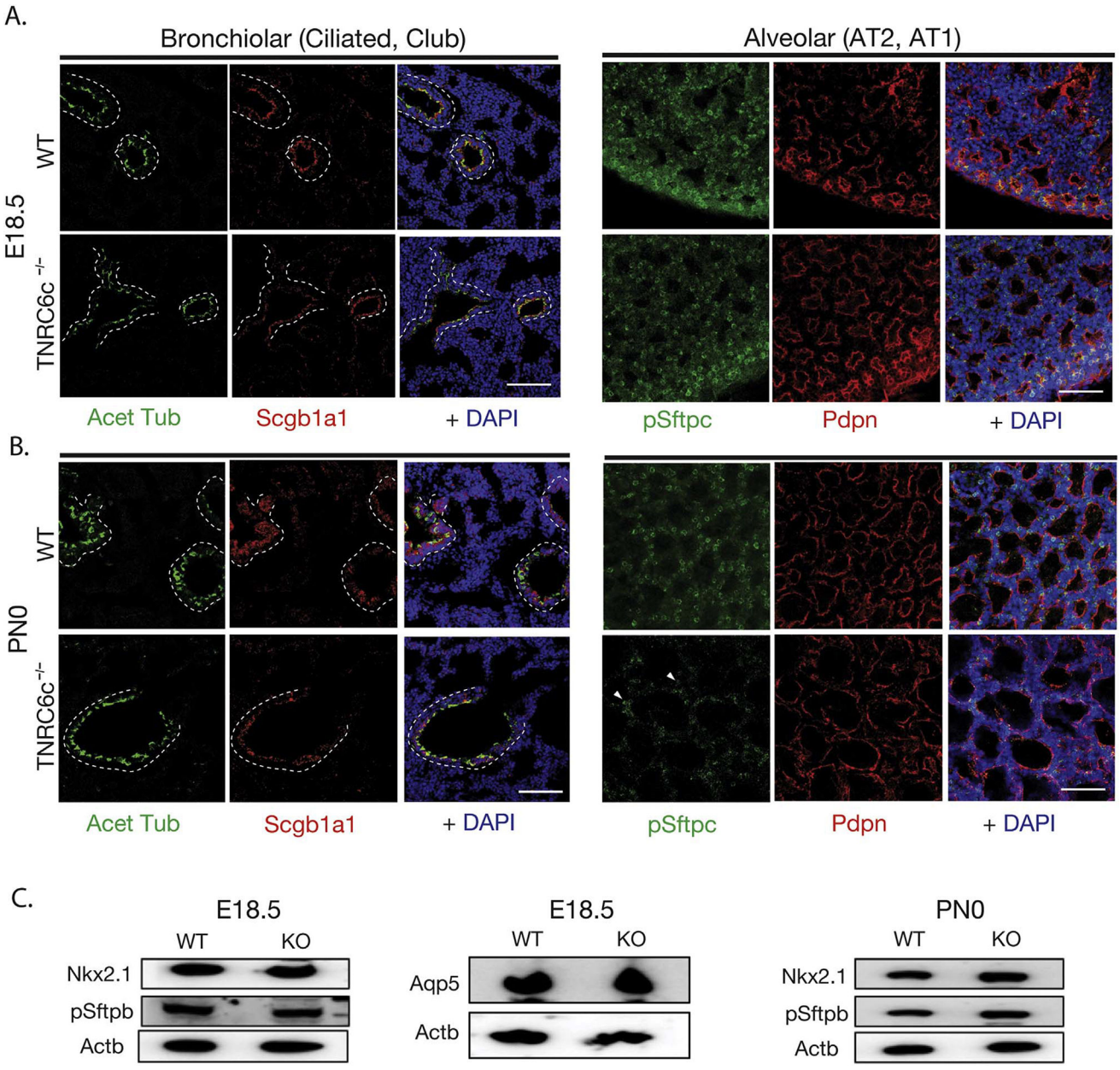

Fig. 2.

Lung epithelial cells in TNRC6c mutants undergo proper histologic and molecular differentiation. A-B. Fluorescent micrographs of lung sections from E18.5 (A) and PN0 (B) WT and TNRC6c null mice immunostained for Club (Secretoglobin 1a1, Scgb1a), ciliated (acetylated tubulin, Acet Tub), AT2 (pro-Surfactant protein C, pSftpc) and AT1 (Podoplanin, Pdpn) cell type markers along with nuclear counterstain (DAPI). Note appropriate localization of airway (Club, ciliated) and gas exchange (AT1, AT2) epithelial cell types in bronchioles (outlined by white dashed line) and distal saccules, respectively. AT2 cells (pSftpc+) are present at E18.5 along with flat AT1 cells (Pdpn+), but exhibit reduced levels of pSftpc staining at PN0 (white arrowheads) in TNRC6c mutants compared with WT and E18.5 mutant lungs. C. Western blots for Nkx2.1 (NK2 Homeobox 1;

Author Manuscript Author Manuscript Author Manuscript Author Manuscript

epithelial cells), pSftpB (pro-Surfactant protein B; mature AT2 cells), and Aqp5 (Aquaporin 5; mature AT1 cells) along with Actb (beta actin) at E18.5 and PN0. Note similar levels of expression in mutant and WT lungs. Scale bar, 100 μm. AT, alveolar epithelial type; E, embryonic day; PN, postnatal day; WT, wild type.

Author Manuscript Author Manuscript Author Manuscript Author Manuscript

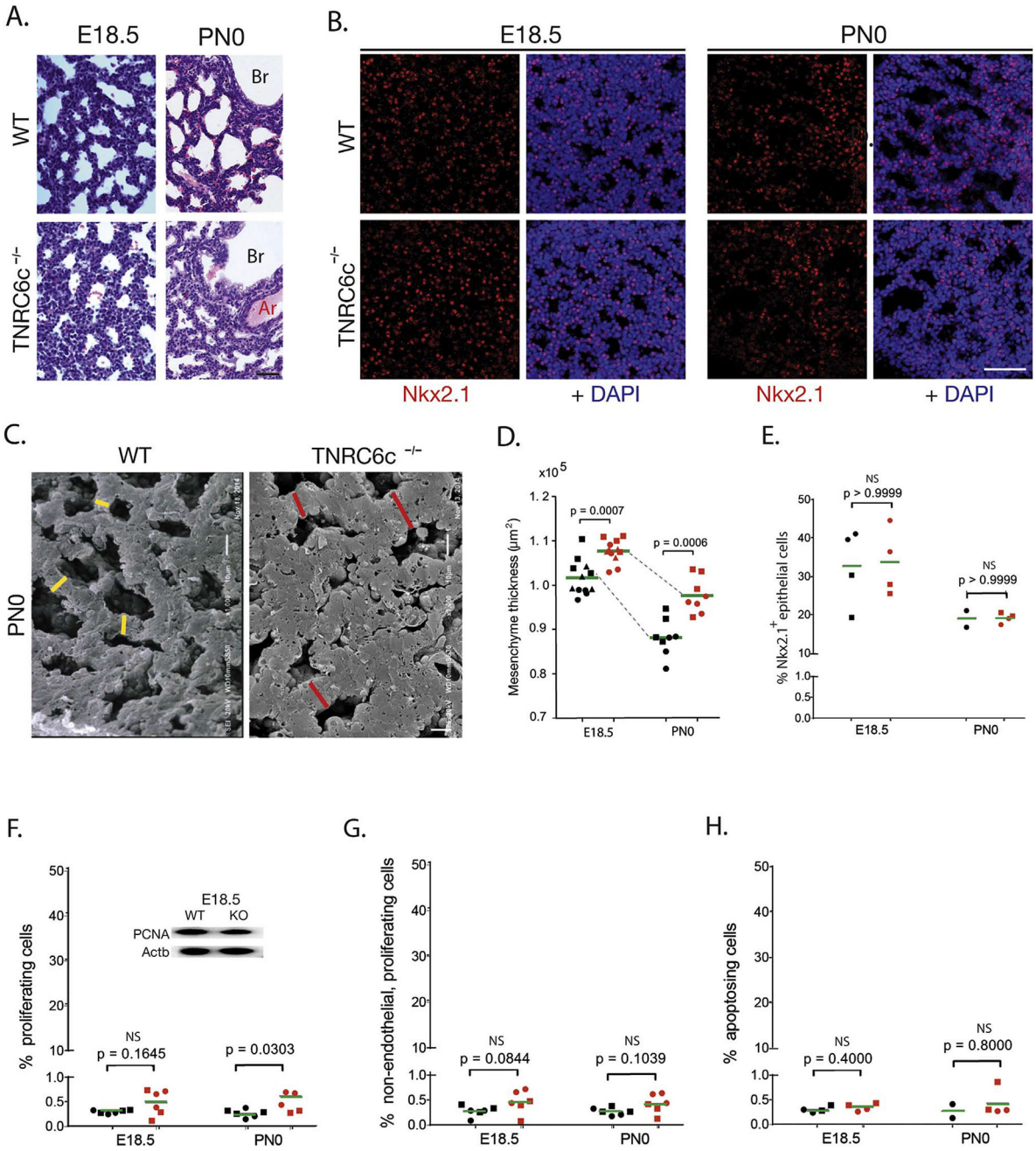

Fig. 3.

TNRC6c null mutants undergo incomplete mesenchymal thinning but maintain proper epithelial cell proportions and kinetics during sacculation. A. H & E of WT and TNRC6c null lungs at E18.5 and PN0. Note mutant mesenchyme is thicker than WT at E18.5, with evidence of only partial thinning compared with WT at PN0. Scale bar, 50 μm. B. Fluorescent micrographs of distal lung from WT and TNRC6c null mice at E18.5 (left) and PN0 (right) immunostained for epithelial cells (NK2 Homeobox 1, Nkx2.1) and nuclear counterstain (DAPI). Note similar salt and pepper distribution of epithelial cell nuclei in WT and mutant lungs. Scale bar, 50 μm. C. SEM of distal lung at PN0 shows TNRC6c null

Author Manuscript Author Manuscript Author Manuscript Author Manuscript

mutant air sacs are smaller and thicker-walled compared with WT littermate. Thickness of several primary septae between adjacent air sacs indicated by yellow (WT) and red (null mutant) lines. Scale bar, 10 μm. D. Quantification of air sac mesenchyme thickness in TNRC6c mutant (red) and WT (black) littermates, showing incomplete thinning in mutants between E18.5 and PN0. E. Percentage of distal lung epithelial (Nkx2.1+) cells at E18.5 and PN0 shows no difference between WT and mutant. F-G. Similar levels of PCNA (proliferating cell nuclear antigen) at E18.5 (Western blot, F, inset) and low percentage of proliferating (MKi67+) total (F, graph) and non-endothelial (G) cells at E18.5 and PN0 in mutant and WT distal lung. Actb, beta actin. H. Low percentage of cells undergoing apoptosis (cleaved Caspase 3+) at E18.5 and PN0 in WT and mutant distal lung. For D-H, each symbol indicates a distinct data point and each shape a different animal. Horizontal bars indicate the mean value. p-values were calculated with the Wilcoxon Rank Sum test. Ar, pulmonary artery; Br, bronchus; E, embryonic day; H & E, hematoxylin and eosin; NS, non-significant; PN, postnatal day; SEM, scanning electron microscopy; WT, wild type.

Author Manuscript
Author Manuscript
Author Manuscript
Author Manuscript

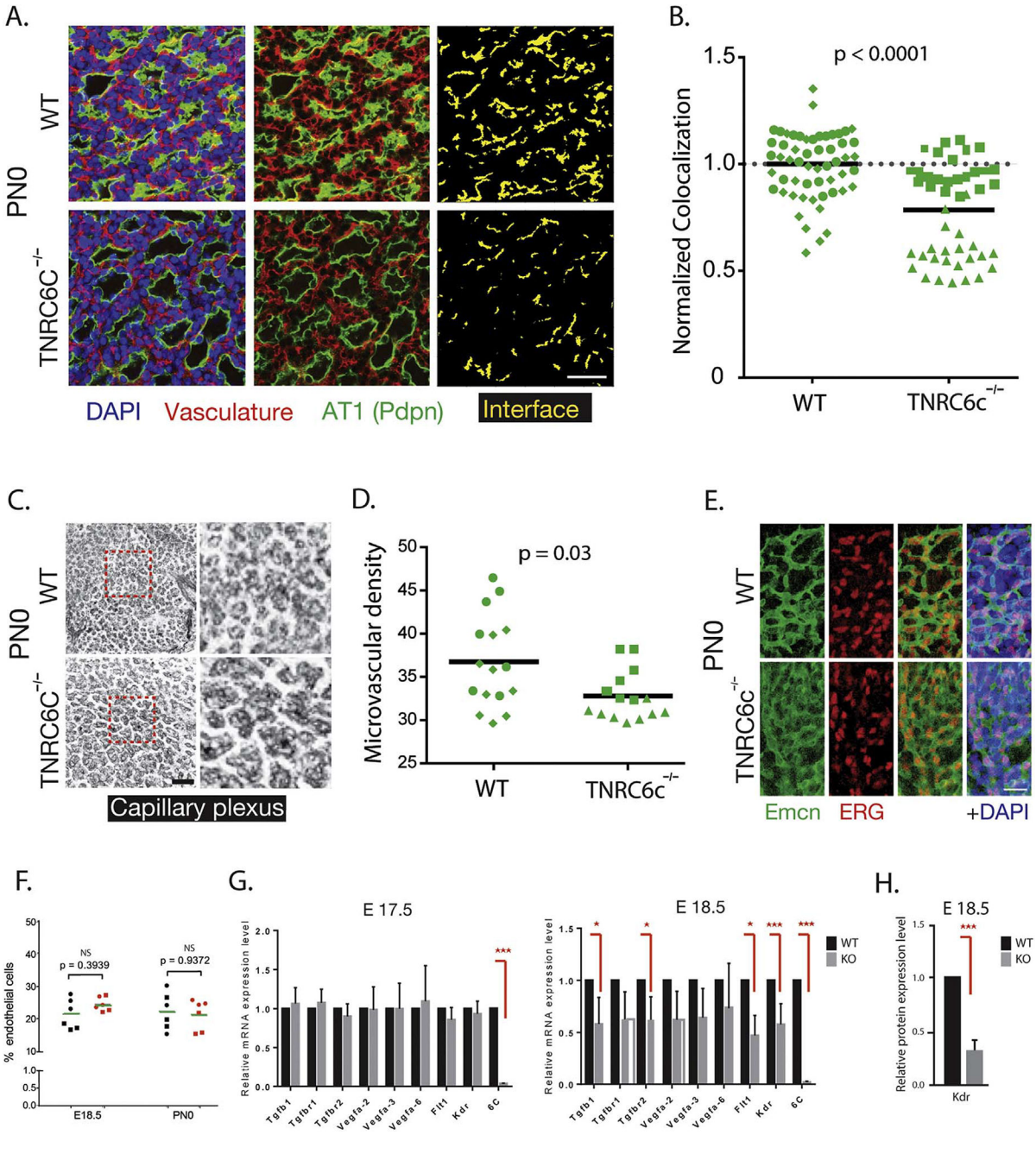

Fig. 4.

Microvascular immaturity with dynamically reduced expression of TGF beta and VEGF family genes in TNRC6c mutant lungs. A. Representative images of WT and TNRC6c null mutant distal lung regions showing epithelial surface (green; Pdpn, AT1 cells), vasculature (red; endothelial “cocktail”), and nuclei (blue; DAPI) at PN0 (left panel), and without DAPI to highlight AT1 (green) and endothelial (red) cells (middle panel). Pixels representing areas of AT1-endothelial colocalization (yellow, right panel) obtained by element-wise multiplying of thresholded epithelial and vascular pixels in WT and TNRC6c micrographs. Scale bar, 40 μm. B. Plot showing quantification of AT1-endothelial cell colocalization

Author Manuscript Author Manuscript Author Manuscript Author Manuscript

in WT and TNRC6c null mutant animals at PN0. C. Representative maximum intensity projections of 5 optical slices of WT and TNRC6c null distal lung vasculature (endothelial "cocktail") at PN0 shows simple mesh in mutants with absence of fine projections. Boxed regions in left panels are shown magnified in right panels. Scale bar, 100 μm. D. Data quantifying the microvascular density of WT and TNRC6c lungs, showing significantly reduced density in mutant lungs. E. Representative projection of micrograph of endothelial cells at PN0 in WT and mutant distal lung, immunostained for surface (Endomucin, Emcn) and nuclear (ETS related gene, ERG) markers along with nuclear counterstain (DAPI). Scale, 50 μm. F. Percentage of distal alveolar endothelial cells (ERG+) in WT and mutant lungs at E18.5 and PN0. G. Quantification by qRT-PCR of expression of TGFβ and VEGF family genes in lungs of WT and TNRC6c mutants at E17.5 and E18.5. Note no significant difference between WT and TNRC6c null lungs at E17.5, with dynamic reduction in expression of TGFβ1 and TGFβR2, and of Flt1 and Kdr, at E18.5 in mutants. H. Western Blot for Kdr shows significant reduction in mutant compared with WT lung at E18.5. * indicates $p < 0.05$, *** indicates $p < 0.001$, In B, D, F, each symbol indicates a distinct data point and each shape represents an individual animal. Horizontal bars indicate the mean value, and p-value was calculated with the Wilcoxon Rank Sum test. AT, alveolar epithelial type; E, embryonic day; KO, knockout; NS, non-significant; PN, postnatal day; TGFβ, Transforming Growth Factor beta; VEGF, Vascular Endothelial Growth Factor; WT, wild type.